

This Page Is Inserted by IFW Operations
and is not a part of the Official Record

BEST AVAILABLE IMAGES

Defective images within this document are accurate representations of the original documents submitted by the applicant.

Defects in the images may include (but are not limited to):

- BLACK BORDERS
- TEXT CUT OFF AT TOP, BOTTOM OR SIDES
- FADED TEXT
- ILLEGIBLE TEXT
- SKEWED/SLANTED IMAGES
- COLORED PHOTOS
- BLACK OR VERY BLACK AND WHITE DARK PHOTOS
- GRAY SCALE DOCUMENTS

IMAGES ARE BEST AVAILABLE COPY.

**As rescanning documents *will not* correct images,
please do not report the images to the
Image Problem Mailbox.**

1

Processing and crystallisation of rapidly solidified $\text{Al}_2\text{O}_3\text{-Y}_2\text{O}_3$ fibres

E. A. Aguilar, R. A. L. Drew, B. Saruhan, C. Milz, and B. Hildmann

Amorphous fibres of the $\text{Al}_2\text{O}_3\text{-Y}_2\text{O}_3$ system were prepared by a melt extraction technique, and subjected to crystallisation. The quality of the melt extracted fibres is controlled by the wheel edge and rotational speed, with both having a significant effect on fibre diameter and avoidance of irregularities and instabilities along the fibre length. Tensile strength in the glassy state varied from 0.6 to 1.0 GPa. Crystallisation activation energies calculated from scan-rate dependence of DTA peaks are 741 and 1374 kJ mol^{-1} for E1 ($\text{Al}_2\text{O}_3\text{-yttrium aluminium garnet (YAG) eutectic}$), 390 kJ mol^{-1} for YAG, and 438 kJ mol^{-1} for E2 ($\text{YAG-yttrium aluminium perovskite (YAP) eutectic}$) by the Kissinger method; and 698 and 1346 kJ mol^{-1} for E1, 352 kJ mol^{-1} for YAG, and 399 kJ mol^{-1} for E2 by the Augis-Bennett method. BCT/438

Dr E. A. Aguilar and Dr R. A. L. Drew are in the McGill University, 3610 University, H3A 2B2, Montreal, Qc., Canada. Dr B. Saruhan, Dr C. Milz, and Dr B. Hildmann are in the DLR, Porz-Wahnheide, Linder-Höhe, D-51147, Cologne, Germany. Presented at the 6th Conference and Exhibition of the European Ceramic Society, held at the Brighton Conference Centre, UK, on 20–24 June 1999. Manuscript received 1 June 2000; in final form 17 October 2000.

© 2000 IoM Communications Ltd.

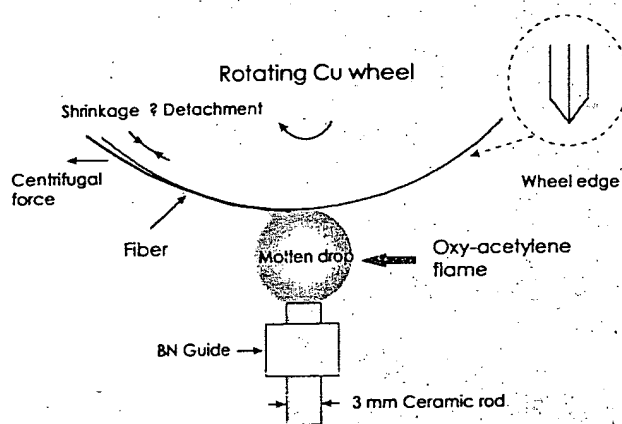
INTRODUCTION

Over the last 25 years great progress has been made in the development of high performance materials. One of the important reasons for this has been the production of ceramic fibres with high tensile strength and modulus values as well as resistance to high temperature. High stiffness oxide fibres such as aluminium and high alumina based fibres are used as reinforcement fibres for production of polymeric, metallic, and ceramic matrix composites with superior properties which have created new engineering possibilities. Those fibres with large additions of silica (aluminosilicate fibres, e.g. Fiberflax, Nextel, etc.) that have low thermal conductivity, low heat capacity, and high chemical resistance are attractive as insulation materials in metal processing industries, where they are frequently used as insulation in furnaces.^{1,2}

There are a variety of techniques for the manufacture of oxide fibres including slurry and sol-gel processing, and inviscid melting. The present study will discuss the fibre forming technique using inviscid melt extraction of $\text{Al}_2\text{O}_3\text{-Y}_2\text{O}_3$ liquids and describe the crystallisation behaviour of the various compositions studied. A novel melt extraction technique³⁻⁵ that has been developed to produce various oxide fibres will be used.

EXPERIMENTAL PROCEDURES

Several compositions may be melt extracted in the $\text{Al}_2\text{O}_3\text{-Y}_2\text{O}_3$ system, however the compositions of interest



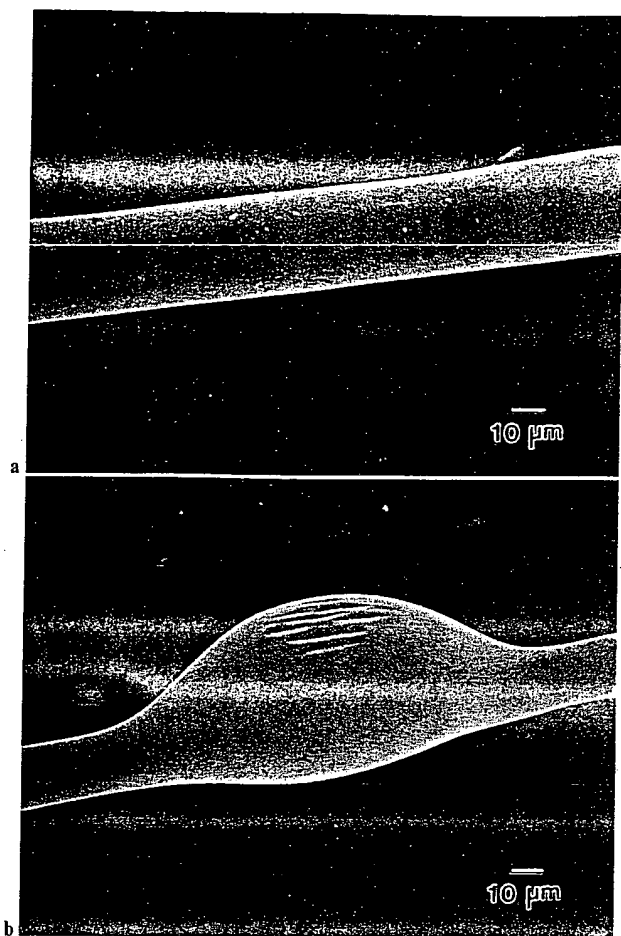
1 Schematic diagram of apparatus for melt extraction

are mainly those based on the alumina rich section of the phase diagram.^{6,7} Three different compositions were investigated: $\text{Al}_2\text{O}_3\text{-YAG}$ eutectic (E1) and 79 mol.-% Al_2O_3 ; yttrium aluminium garnet (YAG) at 62.5 mol.-% Al_2O_3 , and a YAG-yttrium aluminium perovskite (YAP) eutectic (E2), with 57.5 mol.-% Al_2O_3 . Starting materials consisted of aluminium oxide (A17, Alcoa Industrial Chemical Division, 99.5% purity) and yttrium oxide (Grade 5600, Union Molycorp, 99.99% purity).

Melt extraction involves bringing the edge of a rotating disk into contact with a molten ceramic drop. The material solidifies on the disk edge, adheres there briefly, then is spontaneously released in the form of solid fibre. Figure 1 shows a schematic diagram of the apparatus used for making ceramic fibres. The material to be extracted is introduced on to the sharpened wheel (with a radius of curvature of $\approx 20 \mu\text{m}$) from below. The ceramic is first formed into a sintered rod of about 3 mm dia. The rod passes through a loosely fitting guide made of a suitable insulating material (boron nitride) and is then heated by an oxy-acetylene flame to form a small drop which is self-contained by surface tension. The droplet is then slowly pushed towards the rotating wheel to provide a fine contact between the wheel tip and molten drop. On contact with the wheel, the fibre forms and rapidly solidifies. The wheel itself should be made of a reasonably durable metal of good thermal conductivity. Copper-beryllium alloy (C17510) has been found to be satisfactory in the extraction of ceramics.

Melt extracted fibres were studied by scanning electron microscopy to investigate the fibre geometry and morphology. The degree of crystallinity of fibres was examined by XRD analysis of crushed fibres using $\text{Cu K}\alpha$ radiation (at 40 kV and 20 mA). Diffraction patterns were recorded in step-scan mode ($0.02^\circ 2\theta$ intervals, 0.5 s sampling time) over a range $10\text{--}90^\circ 2\theta$. The mechanical properties of uniform diameter fibres were tested using a universal test machine according to ASTM standard D3379-75.

The differential thermal analysis (DTA) measurements (DTA7 Perkin-Elmer) were performed using a constant weight of 40 mg of fibres in an alumina crucible under an



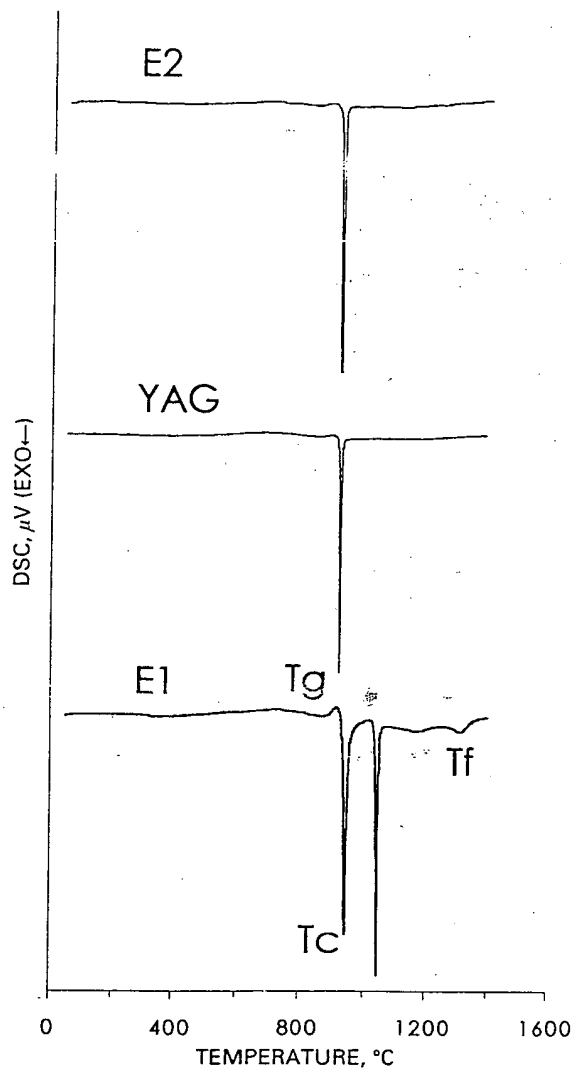
2 Melt extracted fibres of Al_2O_3 -YAG eutectic composition: *a* uniform cross-section fibre; *b* fibre exhibiting Rayleigh waves

argon atmosphere. Alumina powder was used as a reference material. Constant heating rates of 3, 5, 10, 20, 40, and 80 K min^{-1} for E1, and 30, 40, 60, 80, and 100 K min^{-1} for YAG and E2 were used from 750 to 1400°C. Prior to measurement, the temperatures of the DTA were calibrated using aluminium ($\text{Al} > 99.9\%$, mp = 660.10°C) and gold ($\text{Au} > 99.9\%$, mp = 1063°C) standards.

RESULTS

Generally, two types of fibre were obtained: uniform diameter fibres at wheel speeds $< 3 \text{ m s}^{-1}$ with average diameter of 20–30 μm (Fig. 2a), and fibres consisting of thin sections of 20–30 μm and periodic Rayleigh waves with diameters of 60–70 μm (Fig. 2b). The presence of Rayleigh waves at higher velocities is due to a thicker liquid layer being extracted from the molten drop than can solidify completely on the wheel surface. Therefore, the effect of surface tension that tends to minimise the surface area causes the formation of waves. Due to the rapid solidification both fibres are completely X-ray amorphous and optically transparent regardless of wheel velocity and chemical composition in the as extracted state.

The average tensile strengths and Young's modulus for uniform cross-section fibres are shown in Table 1. The tensile strength of the fibres decreased as the alumina content increased. It was noted that with a higher content of alumina, the average diameter of the extracted fibres was larger; therefore the flaw population and defect size in the fibres would be greater. It is believed that the addition of yttria into the mixtures decreases the viscosity of the liquid



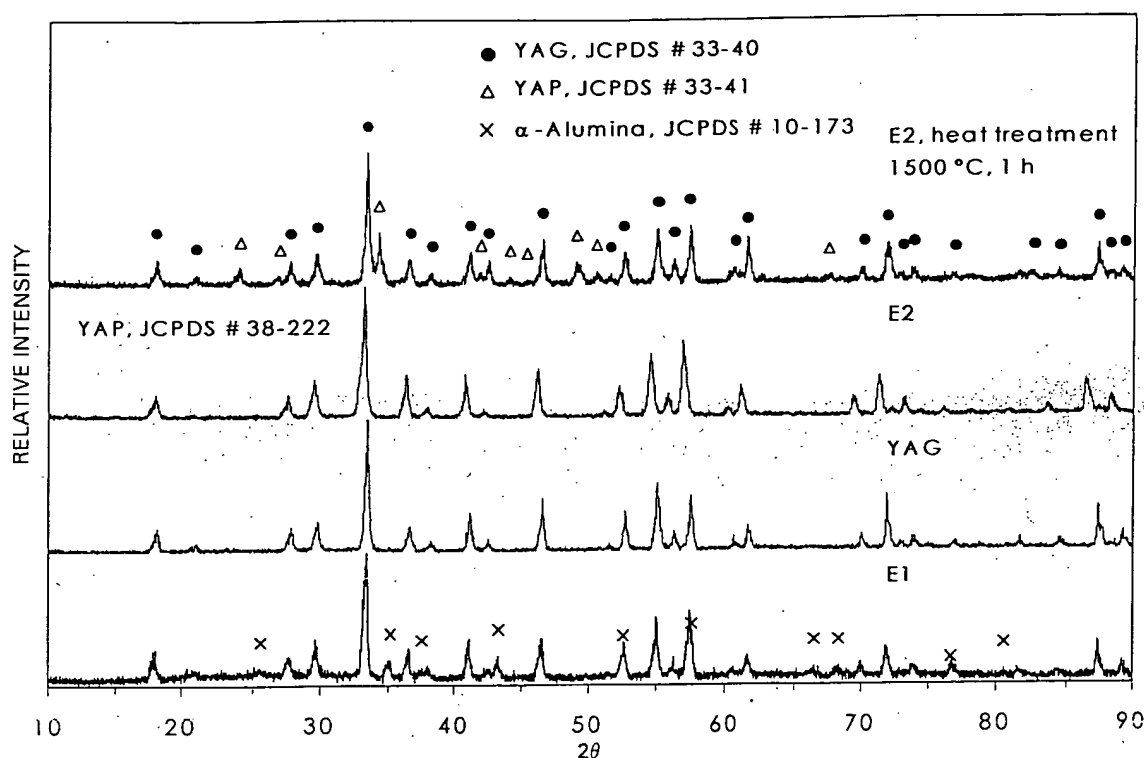
3 Typical DSC for Al_2O_3 - Y_2O_3 fibres at heating rate of 10 K min^{-1}

ceramic facilitating the extraction of a thinner layer on the wheel.

The thermal evolution of glass fibres was followed by means of differential scanning calorimetry (DSC) followed by XRD identification of the resulting phases. Figure 3 shows typical DSC curves for E1, YAG, and E2 fibres at a heating rate of 10 K min^{-1} . The curve is characterised by a small endothermic effect that is due to the glass transition and identified as the T_g temperature. The crystallisation sequence for E1 is characterised by two independent exothermic effects. In order to identify the crystalline phases developed during the DSC treatment, samples were allowed to reach a predetermined temperature associated with the thermal peak and quenched to room temperature for XRD examination. The phases found after each DSC peak were YAG (event 1) and $\delta\text{-Al}_2\text{O}_3$ (event 2). A third small exothermic peak (event 3) was observed around 1300°C correspond-

Table 1 Maximum tensile strengths and average Young's modulus for Al_2O_3 - Y_2O_3

Composition	Tensile strength, MPa	Young's modulus, GPa
E1	949	140
YAG	732	129
E2	565	163



4 XRD of E1, YAG, and E2 fibres after DSC heat treatment at 1400°C

ing to the phase transformation of $\delta\text{-Al}_2\text{O}_3$ to $\alpha\text{-Al}_2\text{O}_3$. The crystallisation sequence for YAG and E2 was characterised by one sharp exothermic peak due to the formation of YAG and YAP (cubic) phases, respectively. These phases are in complete agreement with the equilibrium phase diagram expectations with the exception of E2. The phase development in the E2 composition occurred gradually during heating, forming a sequence of intermediate phases (Fig. 4). Crystallisation began above 900°C and YAP cubic phase formed as the temperature increased. YAP orthorhombic and YAG phases are also apparent at 1400°C. The amount of YAP orthorhombic and YAG phases increased with the temperature and pure YAP orthorhombic and YAG phases formed at 1500°C.

The kinetics of crystallisation of $\text{Al}_2\text{O}_3\text{-Y}_2\text{O}_3$ fibres were obtained by DTA which is a dynamic method. The principle of the continuous heating method assumes that ΔT (the temperature difference between the sample and the standard) is proportional to the crystallisation rate.

The activation energy values for crystallisation were calculated using both the Kissinger (equation (1)),^{8,9} and Augis-Bennett (equation (2))¹⁰ equations by measuring the variation of the peak temperature in the differential thermal patterns with heating rate. Kissinger demonstrated how activation energy and frequency factor could be calculated from DTA experiments in the case of homogeneous solid state reactions following first order kinetics. For that, the decomposition of clay materials in the kaolin group was used. An extension of the Kissinger method applicable to heterogeneous solid state reactions described by an Avrami expression was derived by Augis-Bennett. This new method allowed the study of the kinetics of metallic reactions at the higher temperature obtainable with DTA, such as the transformation kinetics of the metastable equiatomic tin-nickel alloy.

DTA has been used to study the kinetics of rate controlled processes such as the kinetics of crystallisation in glass forming systems. The majority of the data reported have been obtained from DTA measurements on $\text{Li}_2\text{O} \cdot 2\text{SiO}_2$ (Refs. 11-13). The Kissinger equation has been directly

used to examine the activation energy for the crystallisation of amorphous materials such as crystal growth of plasma sprayed cordierite and forsterite,¹⁴ glass-crystal transformation in a CdGeAs glass,¹⁵ and in the phase transition process in glassy $2\text{PbO} \cdot \text{SiO}_2$.¹⁶

Table 2 summarises the crystallisation peak temperatures as a function of heating rate for E1, YAG, and E2 fibres. It can be seen that the faster the scan speed, the higher T_p becomes. A high rate of heating will cause dH/dt to increase because more of the reaction will take place in the same interval of time, and therefore the height or the apex, and the differential temperature ΔT , will be greater. Since the return to the baseline is a time function, as well as a temperature difference function, the return will occur and shift to a higher actual temperature with increasing heating rate ϕ , K min^{-1} (Ref. 17). Therefore Kissinger proposed the following relationship

$$\ln(\theta/T_p^2) = -E_{ck}/RT_p + \text{constant} \quad (1)$$

where E_{ck} is the activation energy for crystallisation, kJ mol^{-1} ; T_p is the absolute crystallisation peak temperature, K; and R is the gas constant $8.314 \times 10^{-3} \text{ kJ mol}^{-1} \text{ K}^{-1}$.

Table 2 Crystallisation peak temperatures T_p for $\text{Al}_2\text{O}_3\text{-Y}_2\text{O}_3$ fibres

Peak temperatures T_p , °C				
ϕ , K min^{-1}	E1, first peak	E1, second peak	YAG	E2
3	922.7	1018.9
5	928.0	1024.9
10	936.0	1031.2
20	948.6	1039.7
30	948.2	947.8
40	959.5	1048.3	955.8	952.4
60	970.3	963.2
80	975.9	1051.0	979.1	973.3
100	984.3	980.0

From the slope of the plot of $\ln(\phi/T_p^2)$ versus $1/T_p$, the E_{ck} value was determined as 741 kJ mol^{-1} and 1374 kJ mol^{-1} for the first and second crystallisation steps, respectively, in the Al_2O_3 -YAG eutectic fibres, and 390 kJ mol^{-1} and 438 kJ mol^{-1} for YAG and YAG-YAP eutectic fibres, respectively. The other method of analysing DTA data proposed by Augis and Bennett is

$$\ln(\phi(T_p - T_0)) = -E_{\text{cab}}/RT_p + \text{constant} \quad (2)$$

where E_{cab} is the activation energy for crystallisation, kJ mol^{-1} ; T_0 the temperature from which the DTA scan starts (here, 1023 K).

The E_{cab} can also be calculated from the slope of $\ln(\phi/(T_p - T_0))$ versus $1/T_p$ plot. The E_{cab} values for Al_2O_3 -YAG eutectic fibres were determined as 698 kJ mol^{-1} and 1346 kJ mol^{-1} for first and second crystallisation steps, respectively. The values of E_{cab} for YAG and YAG-YAP eutectic fibres are 352 kJ mol^{-1} and 399 kJ mol^{-1} , respectively.

Both methods have been applied in the crystallisation of inviscid melt spun calcia-alumina eutectic fibres.¹⁸ The activation energies for crystallisation were determined as 490 and 477 kJ mol^{-1} by Kissinger and Augis-Bennett methods, respectively. These values are in the order of the reported values for the crystallisation of E1 (first peak), YAG, and E2. The high activation energies obtained are probably due to the mechanism of solid state diffusion which may involve the rate at which the irregular glass structure can be rearranged into the periodic lattice of the growing crystal.

CONCLUSIONS

Small diameter (20 – $30 \mu\text{m}$) and moderate strength (0.6 – 1.0 GPa) amorphous alumina-yttria fibres can be obtained using the melt extraction technique. Activation energies for crystallisation of the alumina-yttria fibres were determined as 741 and 1374 kJ mol^{-1} for the Al_2O_3 -yttrium aluminium garnet (YAG) eutectic (E1), 390 kJ mol^{-1} for YAG, and 438 kJ mol^{-1} for the YAG-yttrium aluminium perovskite (YAP) eutectic E2 via the Kissinger method; and

as 698 and 1346 kJ mol^{-1} for E1, 352 kJ mol^{-1} for YAG, and 399 kJ mol^{-1} for E2 via the Augis-Bennett method.

ACKNOWLEDGEMENTS

The authors wish to thank CONACYT (Consejo Nacional de Ciencia y Tecnología, Mexico) for granting a scholarship to E. A. Aguilar and NSERC (The Natural Sources and Engineering Research Council of Canada) for partial funding of this project.

REFERENCES

1. K. K. CHAWLA: 'Fibrous materials', 1st edn; 1998, Cambridge, UK, Cambridge University Press.
2. T. F. COOKE: *J. Am. Ceram. Soc.*, 1991, **74**, (12), 2959–2978.
3. J. O. STROM-OLSEN and P. Z. RUDKOWSKI: 'Apparatus and method for fabrication of metallic fibers having a small cross section', US patent no. 5027886, July 2, 1991.
4. J. STROM-OLSEN: *Mater. Sci. Eng.*, 1994, **A178**, 239–243.
5. J. O. STROM-OLSEN, G. RUDKOWSKA, P. RUDKOWSKI, M. ALLAHVERDI, and R. A. L. DREW: *Mater. Sci. Eng.*, 1994, **A179/A180**, 158–162.
6. R. S. ROTH: 'Phase equilibria diagrams', Phase Diagrams for Ceramists, Vol. XI, 107; 1995, Westerville, OH, American Ceramic Society.
7. G. T. ADYLOV, G. V. VORONOV, E. P. MANSUROVA, L. M. SIGALOW, and E. M. URAZAEVA: *Russ. J. Inorganic Chem.*, 1988, **33**, (7), 1062–1063.
8. H. E. KISSINGER: *J. Res. Natl. Bur. Stand.*, Oct. 1956, **57**, (4), 217–221.
9. H. E. KISSINGER: *Anal. Chem.*, Nov. 1957, **29**, (11), 1702–1706.
10. J. A. AUGIS and J. E. BENNETT: *J. Therm. Anal.*, 1978, **13**, 283–292.
11. C. S. RAY and D. E. DAY: *J. Am. Ceram. Soc.*, 1990, **73**, (2), 439–442.
12. C. S. RAY, W. HUANG, K. L. NARAYAN, T. S. CULL, and K. F. KELTON: *J. Non-Cryst. Solids*, 1996, **204**, 1–12.
13. W. F. HAMMETTER and R. E. LOEHMAN: *J. Am. Ceram. Soc.*, 1987, **70**, (8), 577–582.
14. H. G. WANG, H. HERMAN, and X. LIU: *J. Mater. Sci.*, 1990, **25**, 2339–2343.
15. S. RISBUD: *J. Am. Ceram. Soc.*, 1973, **56**, (8), 440–441.
16. J. GÖTZ: *Phys. Chem. Glasses*, 1997, **18**, (2), 32–35.
17. W. W. M. WENDLANDT: 'Thermal analysis', 3rd edn; 1986, New York, Wiley.
18. Y.-M. SUNG, S. A. DUNN, and J. A. KOUTSKY: *Chem. Int.*, 1995, **21**, 169–172.